HHS Public Access

Author manuscript

Radiother Oncol. Author manuscript; available in PMC 2018 August 01.

Published in final edited form as:

Radiother Oncol. 2017 August ; 124(2): 248–255. doi:10.1016/j.radonc.2017.07.017.

Patterns-of-failure guided biological target volume definition for Head and Neck cancer patients: FDG-PET and dosimetric analysis of dose escalation candidate subregions

Abdallah S. R. Mohamed, M.D., M.Sc.[1,4,*], **Carlos E Cardenas, M.S.**[2,*], **Adam S. Garden, M.D.**[1], **Musaddiq J. Awan, M.D.**[5], **Crosby D. Rock, BS**[1], **Sarah A. Westergaard, BS**[1], **G. Brandon Gunn, MD**[1], **Abdelaziz M. Belal, MD, PhD**[4], **Ahmed G. El-Gowily, MD, PhD**[4], **Stephen Y. Lai, MD**[3], **David I. Rosenthal, M.D.**[1], **Clifton D. Fuller, M.D., PhD**[1,^], and **Michalis Aristophanous, PhD**[2,^]

[1]Department of Radiation Oncology, The University of Texas MD Anderson Cancer Center, Houston, TX, USA

[2]Department of Radiation Physics, The University of Texas MD Anderson Cancer Center, Houston, TX, USA

[3]Department of Head and Neck Surgery, The University of Texas MD Anderson Cancer Center, Houston, TX, USA

[4]Department of Clinical Oncology and Nuclear Medicine, Faculty of Medicine, University of Alexandria, Alexandria, Egypt

[5]Department of Radiation Oncology, Case Western Reserve University, Cleveland, OH, USA

Abstract

Background—To identify the radio-resistant subvolumes in pretreatment FDG-PET by mapping the spatial location of the origin of tumor recurrence after IMRT for head-and-neck squamous cell cancer to the pretreatment FDG-PET/CT.

Methods—Patients with local/regional recurrence after IMRT with available FDG-PET/CT and post-failure CT were included. For each patient, both pre-therapy PET/CT and recurrence CT were co-registered with the planning CT (pCT). A 4-mm radius was added to the centroid of mapped recurrence growth target volumes (rGTV's) to create recurrence nidus-volumes (NVs). The overlap between boost-tumor-volumes (BTV) representing different SUV thresholds/margins combinations and NVs was measured.

^Co-Corresponding author: Clifton D. Fuller, MD, PhD, Head and Neck Section, Department of Radiation Oncology, Unit 97, The University of Texas MD Anderson Cancer Center, 1515 Holcombe Boulevard, Houston, Texas 77030, USA. Phone: 713-563-2334, Fax: 713-563-2366, cdfuller@mdanderson.org AND Michalis Aristophanous, PhD, Department of Radiation Physics, The University of Texas MD Anderson Cancer Center, 1515 Holcombe Boulevard, Houston, Texas 77030, USA. MAristophanous@mdanderson.org.
*Equal contribution

Conflict of interest statement:
The authors declare no conflicts of interest.

Results—Forty-seven patients were eligible. Forty-two (89.4%) had type A central high dose failure. Twenty-six (48%) of type A rGTVs were at the primary site and 28 (52%) were at the nodal site. The mean dose of type A rGTVs was 71 Gy. BTV consisting of 50% of the maximum SUV plus 10mm margin was the best subvolume for dose boosting due to high coverage of primary site NVs (92.3%), low average relative volume to CTV1 (41%), and least average percent voxels outside CTV1 (19%).

Conclusions—The majority of loco-regional recurrences originate in the regions of central-high-dose. When correlated with pretreatment FDG-PET, the majority of recurrences originated in an area that would be covered by additional 10 mm margin on the volume of 50% of the maximum FDG uptake.

Keywords

FDG-PET; Patterns of Failure; Dose escalation; Biological Target Volume; Head and Neck Cancer

Introduction

Despite recent advances in radiation therapy (RT), such as intensity modulated radiotherapy (IMRT) and image guided radiotherapy (IGRT), local and/or regional tumor recurrence is still the major mode of therapy failure for head and neck squamous cell cancer (HNSCC) patients [1–4]. Identifying areas at higher risk of recurrence within gross target volume (GTV) with subsequent dose escalation represents a promising strategy towards reducing the rate of locoregional disease failure. [5–12]

Dose escalation in HNSCC is, nonetheless, limited by the proximity of multiple critical normal tissues. A strategy to target smaller radio-resistant subvolumes of the gross disease with higher radiation dose would be more safe and successful if the precise identification of these subvolumes is feasible. Biological imaging modalities are promising for the creation of more spatially accurate maps of radio-resistant sub-regions of the disease compared with standard anatomical modalities. ^{18}F-fluorodeoxyglucose positron emission tomography (FDG-PET) is the most widely utilized biological imaging modality in the clinical setting. Dose escalation strategies based on FDG-PET imaging are emerging in multiple cancer subsites. [13]

However, only a few HNSCC dose escalation clinical trials have been undertaken. In those early phase trials, the definition of FDG-PET guided dose escalation sub-volumes had been variable. The authors of the ARTFORCE phase II study designed their dose escalation sub-volumes based on 50% of the maximum uptake in the primary tumor plus a 3 mm margin to create a final PTV-FDG-PET.[14] Investigators from Ghent University Hospital implemented different strategies in two phase I dose escalation studies, using focal dose painting by contours based on the source-to-background ratio in one study[15] and dose painting by number in the second study.[16]

The rationale of defining distinct FDG-PET standard uptake value (SUV) levels as a threshold to dose escalate GTV subvolumes in HNSCC trials has not been validated in large scale datasets and mainly has been extrapolated from non-head and neck subsites (e.g. a

non-small cell lung cancer study showed that the 50% SUV high FDG uptake area of the pre-radiotherapy scan overlapped significantly with the residual metabolically active areas post-treatment).[17] The identification of “evidence-based” pretreatment FDG-PET sub-volumes to guide future dose escalation studies is still an unmet need in HNSCC.

To this end, we aim to map the spatial location of the origin of posttreatment tumor recurrence to the pretreatment FDG-PET/CT in a large scale post-IMRT HNSCC failure dataset using a quality assured deformable image registration methodology. We sought the following specific aims:

1. Identify the geometric origin of local and/or nodal recurrence relative to the pretreatment FDG-PET scan and relative to the original treatment target volumes.
2. Identify FDG-PET SUV thresholds that overlap with the majority of tumor recurrences’ origin.
3. Determine the most feasible FDG-PET boost volume with the most overlap with recurrences’ origin and with the smallest size relative to high dose clinical target volumes (CTVs).
4. Generate hypotheses for future FDG-PET based dose escalation clinical trials in HNSCC.

Materials and Methods

Patient population

Patients with local and/or regional recurrence after curative-intent IMRT for HNSCC between January 2006 and August 2010 were identified under an institutional review board (IRB) approved protocol. Conditions for patient eligibility included:

1. Pathologically (histologically/cytologically) proven diagnosis of HNSCC.
2. Pathologic and/or radiologic evidence of local and/or regional recurrence after treatment.
3. Available pre-IMRT FDG PET/CT scan and retrievable IMRT plans.
4. Available CT scan of failure site prior to any salvage therapy.
5. Patients with previous radiation to the head and neck area or synchronous cancer were excluded.

IMRT Treatment Planning and Delivery

All patients had been positioned supine in an individualized thermoplastic head and shoulder mask for CT simulation and treatment and a custom dental stent used as an intraoral immobilization and displacement device. A treatment planning CT (pCT) scan was used for defining target volumes (TVs). TV definition was done in the Pinnacle treatment planning system (Pinnacle, Phillips Medical Systems, Andover, MA), with rigorous multi-physician quality assurance.[18]

Treatment was uniformly delivered by linear accelerators using 6-MV photons. Three clinical target volumes (CTV) had been defined: CTV1, which included gross tumor volume (GTV) plus margin, where GTV included all known gross disease (primary tumor plus grossly enlarged lymph nodes); CTV2, which included the mucosal, bony, and nodal volumes at intermediate risk of harboring microscopic disease; CTV3, which included the mucosal, bony, and nodal volumes at low risk of harboring microscopic disease. IMRT was delivered in 33–35 fractions. The dose prescribed to CTV1 was 66–70Gy, the dose prescribed to CTV2 ranged from 60–63 Gy and the dose prescribed to CTV3 ranged from 56–57 Gy. The prescribed dose to the uninvolved low-neck field was 50 Gy in 25 fractions. Each Planning Target Volume (PTV) was defined as the CTV plus 3–4 mm margin, with daily IGRT[19]. Patients were treated using a monoisocentric technique with an antero-posterior low-neck supraclavicular field matched to the IMRT fields or using whole neck IMRT for cases where gross nodes were located at the match line.

Loco-regional Recurrence

Cases where local and/or regional recurrent disease were recorded had their post-failure/pre-salvage diagnostic images exported as DICOM files from the clinical PACS system to Pinnacle, where radiological evident recurrent gross disease (rGTV) was manually delineated by a radiation oncologist (ASRM) and reviewed by a head and neck service-specific attending radiation oncologist (CDF). The date of failure was defined as the date of first follow-up study indicating recurrent disease.

Image registration

Planning CT (pCT), target volumes, and dose maps were restored for this analysis. The metabolic tumor volume was identified on the pre-radiotherapy FDG-PET scan using an in-house auto-segmentation algorithm (PET-GTV$_{AS}$)[20], which has been optimized and validated for HNSCC [21]. For each patient, both pretreatment FDG-PET/CT and recurrence depicting CT (recCT) were co-registered with pCT scan using a prior validated atlas-based deformable image registration commercial software, ADMIRE version 1.13.5 (ELEKTA, Stockholm, Sweden 2016).[22, 23]

Subsequently, planning CTs; dose grids; original plan target volumes; recurrence CTs; rGTVs; PET-CTs; PET-GTV$_{AS}$; and deformation vector fields were all imported in a custom written Matlab routine (MATLAB R2014b, The MathWorks Inc., Natick, MA, 2014). The deformation vector fields were then applied to PET-GTV$_{AS}$ segmented on PET/CT and rGTV segmented on the recurrence CT to convert them into a deformed PET-GTV$_{AS}$ and a deformed rGTV on the planning CT, respectively. Figure 1 depicts the workflow methodology described above.

Recurrence Origin Mapping

The center of mass of the registered rGTV was identified as the origin from where failure expanded (i.e. nidus of the recurrence) and a nidus volume (NV) was created by adding a 4 mm radius to account for uncertainties in registration and delineation. A margin of 4 mm was decided using error propagation (Eq. 1) [24]of the known uncertainties (2 mm for registration and 3 mm for delineation) providing an overall uncertainty of 3.6 mm that was

rounded to 4 mm. Additional nidus volumes were generated by increasing the radius from 0 to 10 mm, in 2 mm increments, for a comprehensive evaluation of the uncertainty of the nidus (origin of the recurrence). The location of deformed NVs was then compared relative to the deformed PET-GTV_{AS} contours location as well as the original plan target volumes and dose.

$$\delta E = \sqrt{(\delta r)^2 + (\delta d)^2} \quad \text{Eq. 1}$$

Where δr is the uncertainty in registration and δd is the uncertainty in delineation.

Patterns of loco/regional recurrence

Failures were classified according to both geometric and dosimetric criteria as previously described by our group[25]. In brief, the geometric mapping of recurrence origin was done by correlating the NV of each rGTV to the corresponding TV in the planning CT. Subsequently, the dosimetric characteristics were assessed by calculating the dose to 95% of the failure volume (fD95%) then comparing it relative to the dose prescribed to the corresponding TV of origin as determined by the geometric mapping. Finally, failures were classified into five major types: Type A (central high dose where fD95% is ≥95% dose prescribed to corresponding high doseTV of origin), Type B (peripheral high dose where fD95% is <95 % dose prescribed to corresponding high dose TV of origin), Type C (central elective dose where fD95% is ≥95% dose prescribed to corresponding lower dose TV of origin), Type D (peripheral elective dose where fD95% is <95% dose prescribed to corresponding lower dose TV of origin), and Type E (extraneous dose where rGTV centroid originates outside all TVs). Type F describes junctional failures at the IMRT/supraclavicular match line, and Type G describes low neck failures at the low-neck supraclavicular field. The overall pattern of failure for patients with type A recurrence and concurrent non-type A recurrence was defined as type A. While patients who had more than one non-type A at the same time, pattern of failure of each patient was classified according to the most predominant type based on rGTV volume.

PET boost volumes

For this analysis the 30%, 40%, 50%, 60% and 70% of the maximum SUV volumes were identified on the pre-radiotherapy FDG-PET images and an isotropic margin of 0–20mm (in an iterative increments of 2mm) was added around each iso-intensity volume to create boost tumor volumes (BTV30+0, BTV30+2, ..., BTV70+20). For each deformed BTV, the overlap with the 4 mm NV of all recurrence lesions of type A nature was recorded. The BTV was considered adequate to capture the nidus of recurrence if the overlap was greater than 95% provided that BTV volume is less than CTV1 volume. All BTVs with volume ≥ CTV1 volumes were excluded. For primary site recurrences, additional analysis was done to identify the best possible BTV candidate by calculating the percent volume of the selected BTV relative to the high dose CTV (thus minimizing the necessary boost volume). Because the generated margins around BTVs were isotropic in nature, we also calculated the percent of voxels of each boost volume that were outside the high dose CTV (0% is the best and

100% is worst). Lastly, differences in the percent of lesions covered between the 0 and 10 mm margin nidus volumes were used to assess each BTV's robustness to uncertainty in the identification of the nidus. To identify the best possible boost tumor volume, an arbitrary score function (Eq. 2) was determined and scores were calculated for each volume.

$$Score=[\%\,of\ patients\ covered+(Robustness)+(100-\%\,of\ Boost\ Volume\ outside\ CTV1)+(100-\%\,of\ CTV1\ covered\ by\ boost\ volume)]/4$$

Eq. 2

where Robustness = 100 − (% *of* 10 *mm Nvs covered* − % *of* 0 *mm NVs covered*)

Statistical analysis

Statistical assessment and data tabulation was performed using JMP v 11Pro (SAS institute, Cary, NC).

Results

Patients and tumor characteristics

A total of 47 patients were eligible for this analysis. Median age was 59 years (range 33–93). Median time from end of radiation treatment to recurrence was 8 months (range 1–58). The PET-GTV$_{AS}$ had a median volume of 24 cm^3 (range: 3–197) and SUV$_{max}$ for these volumes were found to have a median value of 16 (range 6 – 41). Patient, disease, and treatment characteristics are summarized in table 1.

Patterns of failure

Patients included in this analysis had failure at the primary site in 19 patients (40.4%), at the nodal site in 18 patients (38.3%), and in both the primary and nodal sites in 10 patients (21.3%). Forty-two patients (89.4%) were classified as type A failure. Five patients (10.6%) were of non-type A failure; two were type C, one type D, and one type E.

A total of 66 rGTVs were identified. Median rGTV volume was 3.7 cm^3 (IQR 2–9). Of these, 54 (82%) were of type A, 5 (7.5%) were type C (i.e. central low dose), 1 (1.5%) was type D (i.e. peripheral low dose), 5 (7.5%) were type E (i.e. out of field), and 1 (1.5%) was type G (i.e. in the low neck supraclavicular field). For type A's rGTVs, 26 (48%) were at the primary site and 28 (52%) were at the nodal site. The mean (SD) of mean doses of all rGTVs' originating in high dose regions was 71 Gy (2) and the mean of dose to 95% rGTVs' volume was 69 Gy (3). Figure 2 depicts the patterns of failure classification per patient and per individual recurrence lesion.

PET boost volumes

The range of BTVs that encompasses the recurrence origin (i.e. nidus volume) of all type A rGTVs is listed in Figure 3. PET-GTV$_{AS}$ overlapped with 38% of NVs of the primary sites

and 32% of NVs of the nodal sites. With no added margins, the examined SUV thresholds did not overlap with most of NVs. For example, when no margin expansion is included, BTV50 (i.e. BTV50+0) covered less than 20% of type A primary site's nidus volumes, while lowering the threshold BTV30 only resulted in 50% coverage of primary site recurrence origin. However, with additional margin expansion, more than one BTV alternative resulted in the coverage of ≥90% of the primary site nidus volumes as well as the coverage of ≥75% of all type A nidus volumes as shown in Figure 3.

Nevertheless, as shown in Figure 4, the candidate BTVs with ≥90% of the primary site nidus volumes coverage did not achieve equivalent performance when using the other metrics of best BTV selection (i.e. the percent of BTV volume inside CTV1 relative to the entire CTV1 volume and the percent of voxels outside CTV1). BTV50+10mm had the best collective performance with high NV coverage (92.3%), low average relative volume to CTV1 (41%), least average percent voxels outside CTV1 (19%), and high average robustness metric (i.e. increasing the margin expansion around the rGTV centroid from 0 to 10 mm led to a minor drop in the percent of overlap [27%]). Supplementary figure S1 shows the overall performance score for all BTVs whose volume did not exceed the size of CTV1. As depicted in figure S1, BTV50+10mm outperformed all other volumes based on this criterion. Supplementary figures S2, S3, and S4 show percent of NVs covered per BTV as a function of NV margins.

Figure 5a clearly demonstrates that BTV50+10mm encompasses the vast majority of primary tumor recurrence's origin. While Figure 5b–d depicts a case demonstration of the candidate boost volume relative to recurrence and planning target volumes.

Discussion

The strategy of increasing radiation dose to be delivered to subvolumes of gross tumor with supposed higher radio-resistance while keeping surrounding normal structures at similar or lower dose levels, appears promising as a step towards improving locoregional control and consequently survival in multiple cancer sites.[13, 17, 26] The deployment of such strategy requires optimal integration of spatially accurate biological imaging in radiation treatment paradigms. FDG-PET/CT is a very attractive solution in this context because it is a widely used tracer and a standard of care imaging modality that provides both anatomical as well as biological aspects of tumors (e.g. tumor metabolism).[27–29] FDG-PET/CT has been successfully used for HNSCC radiation treatment planning purposes,[30] however, its effective use for dose escalation requires a validation of the geometric correlation between the origin of posttreatment disease failure, pretreatment FDG-PET uptake, planning target volumes, and radiation dose, which is the main aim of the current study. The uncertainties and limitations of PET are well known[31]. However, they were carefully considered and taken into account in this analysis.

A few prior studies have attempted to address the correlation of patterns of failure to pretreatment FDG-PET for head and neck squamous carcinomas.[32, 33] These studies, however, lacked the validation of the exact spatial correlation between the recurrence's origin and the pretreatment FDG uptake. Such knowledge is required to be able to define the

appropriate subvolumes to target in FDG-PET-guided dose escalation clinical trials. In addition, the number of failures examined in these studies were few. A large scale failure dataset is required to ensure a realistic representation of different patterns of failure encountered clinically. A single previous study by Due et al[34]was the first to attempt to spatially correlate the patterns of failure relative to pretreatment FDG-PET on a cohort of 39 HNSCC recurrences after IMRT. Their results showed that 54% of recurrences were originated inside the FDG-positive volume delineated by the nuclear medicine physician.

In the current study, we used a previously validated deformable image registration software for CT-CT registration in HNSCC[22, 23] to map the segmented recurrence volume in post-failure diagnostic CT back to the simulation CT scan, planning target volumes, and dose grid. Simultaneously, the CT of the pretreatment FDG-PET-CT was also registered to the simulation CT. We used the failure's centroid mapping method proven by prior work from our group and by others [35, 36] as a more discriminative and accurate manner to localize the origins of loco-regional recurrences than volume overlap methods, which may potentially and incorrectly assign recurrences to more peripheral target volumes regions. We added a 4 mm margin expansion of the centroid of the mapped failure volume to create the nidus volume, as the closest approximation of the 3D volume of the recurrence origin and to account for registration and delineation uncertainties.

Our results showed that the majority of patients (89%) failed at the central high dose regions. Surprisingly, as shown in figures 3, 4, and 5a the majority of type A recurrence origin's did not necessarily fall in voxels with the highest uptake of FDG and an additional 10 mm isotropic margin expansion around the 50% of the maximum SUV was required to create a BTV that cover 92% of type A's recurrences at the primary site. Other BTV volumes, though, overlapped with the majority of recurrences. However, those volumes were considered inappropriate for having either larger relative volume compared to CTV1 or higher percent of voxels outside CTV1. BTV50+10mm, on the other hand, had the best collective performance with the highest overlap with a recurrence's origin, the smallest relative volume compared to CTV1 (i.e. realistic boost subvolume), and the least percent of voxels outside CTV1.

These findings show a boost subvolume of 50% of the maximum FDG uptake would cover less than 20% of primary site recurrence's origin. Also, the voxels of highest FDG uptake are not ineluctably the voxels of highest radio-resistance. Thereby, strategies of selective targeting of the voxels of highest uptake by higher dose (e.g. dose painting by number) seem to underestimate the recurrence risk in nearby voxels within the BTV50+10mm which have relatively lower uptake. Consequently, subvolume definition strategies for FDG-PET-guided dose escalation studies should be revised in the context of these findings.

Critically, if we plan to identify regional sub-volume dependent dose modification (e.g. PET-tracer-, MR parameter- or CT-texture-identified "boost" volumes) as a potential modifier of local/regional tumor response, it is imperative that the underlying nomenclature and methodology for defining said events be fully detailed and reproducible. Our attempt, within this dataset, is to not only generate a definitive recommendation for "boostable" subvolume identification, but a methodologic benchmark and process overview for additional

functional/biological/radiomic applications. Conceivably, PET SUV in this manuscript could be replaced in an equivalent analytic framework with multiparametric MRI or radiomic texture profiles. The imperative first step in any of these efforts would be a representational framework, as detailed herein, which adequately describes with known spatial precision quantifiable event probabilities.

Our study, however, does not go without caveats. Being retrospective in nature, the typical limitations of any retrospective study apply. Also, we have assumed that isovolumetric expansion of the recurrence from the center of mass of the recurrence volume would localize the origin of recurrence, which may not be true in all head and neck cancer cases. However, this is the best possible estimation based on empirical findings. We also did a robustness analysis to address the effect of nidus volume on our findings as shown supplemental figure S1–S4. Because of the uncertainties related to non-rigid registration as well as inter-observer contouring variability, we expanded the centroid of recurrence by 4 mm radius as detailed above. This analysis provided additional depth in determining the best available BTVs since it took into consideration the inherent uncertainties presented by arbitrarily choosing a NV with a 4 mm radius. There are many uncertainties associated with the use of FDG-PET[31]. Some of the ones that can influence the identification of the BTV the most are the voxel size ($5.5\times5.5\times3.7mm^3$), the uncertainties related to the reproducibility of SUV_{max} (i.e. 1–6%) [37], as well as blurring due to potential patient motion inherent from the length of the scan. In this work we decided to account for those uncertainties with the combination of different thresholds as a percent of SUV_{max} with different isotropic margins, guided of course as was described in detail by the patterns of failure analysis, combined with an additional robustness analysis of the recurrence centroid. This robustness analysis showed that even with a 10 mm margin expansion around the centroid, BTV50+10mm still covers the majority of primary site recurrences (i.e. >73%).

Nevertheless, this is, to our knowledge, the largest series of HNSCC failure following curative-intent IMRT to robustly and simultaneously characterize the spatial, biological, and dosimetric foci of recurrence in an integrated spatial frame, using a validated pattern of failure methodology. Our data serve to define a candidate BTV volume that appropriately covers the subvolumes of highest radio-resistance based on objective patterns of failure mapping using rigorous image-processing to afford increased spatial certainty as a prior for further investigation and extra-institutional validation.

To conclude, we present 47 HNSCC patients with recurrence following curative intent IMRT. Our results showed that the majority of recurrences occurred in the central high dose regions. When correlated with pretreatment FDG-PET, the majority of these type A recurrences originated in an area that would be covered by a 10 mm margin on the volume of 50% of the maximum FDG uptake. A validation of these findings is needed in multi-institutional and prospective HNSCC treatment failure databases.

Supplementary Material

Refer to Web version on PubMed Central for supplementary material.

Acknowledgments

Funding sources and financial disclosures:

Drs. Lai, Mohamed, and Fuller receive funding support from the National Institutes of Health (NIH)/National Institute for Dental and Craniofacial Research (1R01DE025248-01/R56DE025248-01). Dr. Fuller received grant and/or salary support from the NIH/National Cancer Institute (NCI) Head and Neck Specialized Programs of Research Excellence (SPORE) Developmental Research Program Award (P50CA097007-10) and Paul Calabresi Clinical Oncology Program Award (K12 CA088084-06); the National Science Foundation (NSF), Division of Mathematical Sciences, Joint NIH/NSF Initiative on Quantitative Approaches to Biomedical Big Data (QuBBD) Grant (NSF 1557679); a General Electric Healthcare/MD Anderson Center for Advanced Biomedical Imaging In-Kind Award; an Elekta AB/MD Anderson Department of Radiation Oncology Seed Grant; the Center for Radiation Oncology Research (CROR) at MD Anderson Cancer Center Seed Grant; and the MD Anderson Institutional Research Grant (IRG) Program. Dr. Fuller has received speaker travel funding from Elekta AB. Supported in part by the National Institutes of Health (NIH)/National Cancer Institute (NCI) Cancer Center Support (Core) Grant CA016672 to The University of Texas MD Anderson Cancer Center.

References

1. Chao KS, Ozyigit G, Tran BN, Cengiz M, Dempsey JF, Low DA. Patterns of failure in patients receiving definitive and postoperative IMRT for head-and-neck cancer. Int J Radiat Oncol Biol Phys. 2003; 55:312–21. [PubMed: 12527043]
2. Dawson LA, Anzai Y, Marsh L, Martel MK, Paulino A, Ship JA, et al. Patterns of local-regional recurrence following parotid-sparing conformal and segmental intensity-modulated radiotherapy for head and neck cancer. Int J Radiat Oncol Biol Phys. 2000; 46:1117–26. [PubMed: 10725621]
3. Eisbruch A, Marsh LH, Dawson LA, Bradford CR, Teknos TN, Chepeha DB, et al. Recurrences near base of skull after IMRT for head-and-neck cancer: implications for target delineation in high neck and for parotid gland sparing. Int J Radiat Oncol Biol Phys. 2004; 59:28–42. [PubMed: 15093896]
4. Schoenfeld GO, Amdur RJ, Morris CG, Li JG, Hinerman RW, Mendenhall WM. Patterns of failure and toxicity after intensity-modulated radiotherapy for head and neck cancer. Int J Radiat Oncol Biol Phys. 2008; 71:377–85. [PubMed: 18164838]
5. Berwouts D, Olteanu LAM, Duprez F, Vercauteren T, De Gersem W, De Neve W, et al. Three-phase adaptive dose-painting-by-numbers for head-and-neck cancer: initial results of the phase I clinical trial. Radiotherapy and Oncology. 2013; 107:310–6. [PubMed: 23647760]
6. Chang JH, Wada M, Anderson NJ, Joon DL, Lee ST, Gong SJ, et al. Hypoxia-targeted radiotherapy dose painting for head and neck cancer using F-18-FMISO PET: A biological modeling study. Acta Oncologica. 2013; 52:1723–9. [PubMed: 23317145]
7. Duprez F, De Neve W, De Gersem W, Coghe M, Madani I. Adaptive Dose Painting by Numbers for Head-and-Neck Cancer. International Journal of Radiation Oncology Biology Physics. 2011; 80:1045–55.
8. Grosu A, Piert M, Souvatzoglou M, Wiedenmann N, Machulla H, Pigorsch S, et al. Hypoxia Imaging with 18F-FAZA-PET for dose painting using intensity modulated radiotherapy in patients with head and neck cancer. International Journal of Radiation Oncology Biology Physics. 2005; 63:S132–S3.
9. Houweling AC, Wolf AL, Vogel WV, Hamming-Vrieze O, van Vliet-Vroegindeweij C, de Kamer JBV, et al. FDG-PET and diffusion-weighted MRI in head-and-neck cancer patients: Implications for dose painting. Radiotherapy and Oncology. 2013; 106:250–4. [PubMed: 23395065]
10. Madani I, Duprez F, Boterberg T, Van de Wiele C, Bonte K, Deron P, et al. Maximum tolerated dose in a phase I trial on adaptive dose painting by numbers for head and neck cancer. Radiotherapy and Oncology. 2011; 101:351–5. [PubMed: 21742392]
11. Madani I, Duthoy W, Derie C, De Gersem W, Boterberg T, Saerens M, et al. Positron emission tomography-guided, focal-dose escalation using intensity-modulated radiotherapy for head and neck cancer. International Journal of Radiation Oncology Biology Physics. 2007; 68:126–35.
12. Thorwarth D, Eschmann SM, Paulsen F, Alber M. Hypoxia dose painting based on functional FMISO PET imaging for head-and-neck cancer patients: A feasibility study. International Journal of Radiation Oncology Biology Physics. 2006; 66:S186-S.

13. Shi X, Meng X, Sun X, Xing L, Yu J. PET/CT imaging-guided dose painting in radiation therapy. Cancer Letters. 2014; 355:169–75. [PubMed: 25218590]
14. Heukelom J, Hamming O, Bartelink H, Hoebers F, Giralt J, Herlestam T, et al. Adaptive and innovative Radiation Treatment FOR improving Cancer treatment outcomE (ARTFORCE); a randomized controlled phase II trial for individualized treatment of head and neck cancer. BMC Cancer. 2013; 13:84. [PubMed: 23433435]
15. Madani I, Duthoy W, Derie C, De Gersem W, Boterberg T, Saerens M, et al. Positron emission tomography-guided, focal-dose escalation using intensity-modulated radiotherapy for head and neck cancer. Int J Radiat Oncol Biol Phys. 2007; 68:126–35. [PubMed: 17448871]
16. Duprez F, De Neve W, De Gersem W, Coghe M, Madani I. Adaptive dose painting by numbers for head-and-neck cancer. Int J Radiat Oncol Biol Phys. 2011; 80:1045–55. [PubMed: 20643512]
17. Aerts HJ, van Baardwijk AA, Petit SF, Offermann C, Loon J, Houben R, et al. Identification of residual metabolic-active areas within individual NSCLC tumours using a pre-radiotherapy (18)Fluorodeoxyglucose-PET-CT scan. Radiother Oncol. 2009; 91:386–92. [PubMed: 19329207]
18. Cardenas CE, Mohamed ASR, Tao R, Wong AJR, Awan MJ, Kuruvila S, et al. Prospective Qualitative and Quantitative Analysis of Real-time Peer Review Quality Assurance Rounds Incorporating Direct Physical Examination for Head and Neck Cancer Radiation Therapy. International Journal of Radiation Oncology*Biology*Physics.
19. Zeidan OA, Langen KM, Meeks SL, Manon RR, Wagner TH, Willoughby TR, et al. Evaluation of image-guidance protocols in the treatment of head and neck cancers. International journal of radiation oncology, biology, physics. 2007; 67:670–7.
20. Aristophanous M, Penney BC, Martel MK, Pelizzari CA. A Gaussian mixture model for definition of lung tumor volumes in positron emission tomography. Medical physics. 2007; 34:4223–35. [PubMed: 18072487]
21. Caldas Magalhaes J, Raaijmakers CP, Aristophanous M, Lee JA, Kasperts N, Jager EA, et al. FDG-PET Semi automatic Segmentation Methods for GTV Delineation in Laryngeal and Hypopharyngeal Cancer. International Journal of Radiation Oncology • Biology • Physics. 90:S536.
22. Mohamed ASR, Rosenthal DI, Awan MJ, Garden AS, Kocak-Uzel E, Belal AM, et al. Methodology for analysis and reporting patterns of failure in the Era of IMRT: head and neck cancer applications. Radiation Oncology. 2016; 11:95. [PubMed: 27460585]
23. Mohamed AS, Ruangskul MN, Awan MJ, Baron CA, Kalpathy-Cramer J, Castillo R. Quality Assurance Assessment of Diagnostic and Radiation Therapy-Simulation CT Image Registration for Head and Neck Radiation Therapy: Anatomic Region of Interest-based Comparison of Rigid and Deformable Algorithms. Radiology. 2015:274. [PubMed: 25734550]
24. Bevington, PR. Data Reduction and Error Analysis for the Physical Sciences. New York: McGraw-Hill; 1969.
25. Mohamed AS, Rosenthal DI, Awan MJ, Garden AS, Kocak-Uzel E, Belal AM, et al. Methodology for analysis and reporting patterns of failure in the Era of IMRT: head and neck cancer applications. Radiat Oncol. 2016; 11:95. [PubMed: 27460585]
26. Berwouts D, Olteanu LA, Duprez F, Vercauteren T, De Gersem W, De Neve W, et al. Three-phase adaptive dose-painting-by-numbers for head-and-neck cancer: initial results of the phase I clinical trial. Radiother Oncol. 2013; 107:310–6. [PubMed: 23647760]
27. Das SK, Ten Haken RK. Functional and molecular image guidance in radiotherapy treatment planning optimization. Seminars in radiation oncology. 2011; 21:111–8. [PubMed: 21356479]
28. Phelps ME. Positron emission tomography provides molecular imaging of biological processes. Proceedings of the National Academy of Sciences of the United States of America. 2000; 97:9226–33. [PubMed: 10922074]
29. Dierckx RA, Van de Wiele C. FDG uptake, a surrogate of tumour hypoxia? European Journal of Nuclear Medicine and Molecular Imaging. 2008; 35:1544–9. [PubMed: 18509637]
30. Castelli J, De Bari B, Depeursinge A, Simon A, Devillers A, Roman Jimenez G, et al. Overview of the predictive value of quantitative 18 FDG PET in head and neck cancer treated with chemoradiotherapy. Critical reviews in oncology/hematology. 2016; 108:40–51. [PubMed: 27931839]

31. Boellaard R. Standards for PET image acquisition and quantitative data analysis. Journal of nuclear medicine: official publication, Society of Nuclear Medicine. 2009; 50(Suppl 1):11s–20s.

32. Soto DE, Kessler ML, Piert M, Eisbruch A. Correlation between pretreatment FDG-PET biological target volume and anatomical location of failure after radiation therapy for head and neck cancers. Radiother Oncol. 2008; 89:13–8. [PubMed: 18555547]

33. Dirix P, Vandecaveye V, De Keyzer F, Stroobants S, Hermans R, Nuyts S. Dose painting in radiotherapy for head and neck squamous cell carcinoma: value of repeated functional imaging with (18)F-FDG PET, (18)F-fluoromisonidazole PET, diffusion-weighted MRI, and dynamic contrast-enhanced MRI. Journal of nuclear medicine: official publication, Society of Nuclear Medicine. 2009; 50:1020–7.

34. Due AK, Vogelius IR, Aznar MC, Bentzen SM, Berthelsen AK, Korreman SS, et al. Recurrences after intensity modulated radiotherapy for head and neck squamous cell carcinoma more likely to originate from regions with high baseline [18F]-FDG uptake. Radiotherapy and Oncology. 2014; 111:360–5. [PubMed: 24993331]

35. Due AK, Vogelius IR, Aznar MC, Bentzen SM, Berthelsen AK, Korreman SS. Methods for estimating the site of origin of locoregional recurrence in head and neck squamous cell carcinoma. Strahlenther Onkol. 2012:188.

36. Raktoe SA, Dehnad H, Raaijmakers CP, Braunius W, Terhaard CH. Origin of tumor recurrence after intensity modulated radiation therapy for oropharyngeal squamous cell carcinoma. International journal of radiation oncology, biology, physics. 2013:85.

37. Schwartz J, Humm JL, Gonen M, Kalaigian H, Schoder H, Larson SM, et al. Repeatability of SUV measurements in serial PET. Medical physics. 2011; 38:2629–38. [PubMed: 21776800]

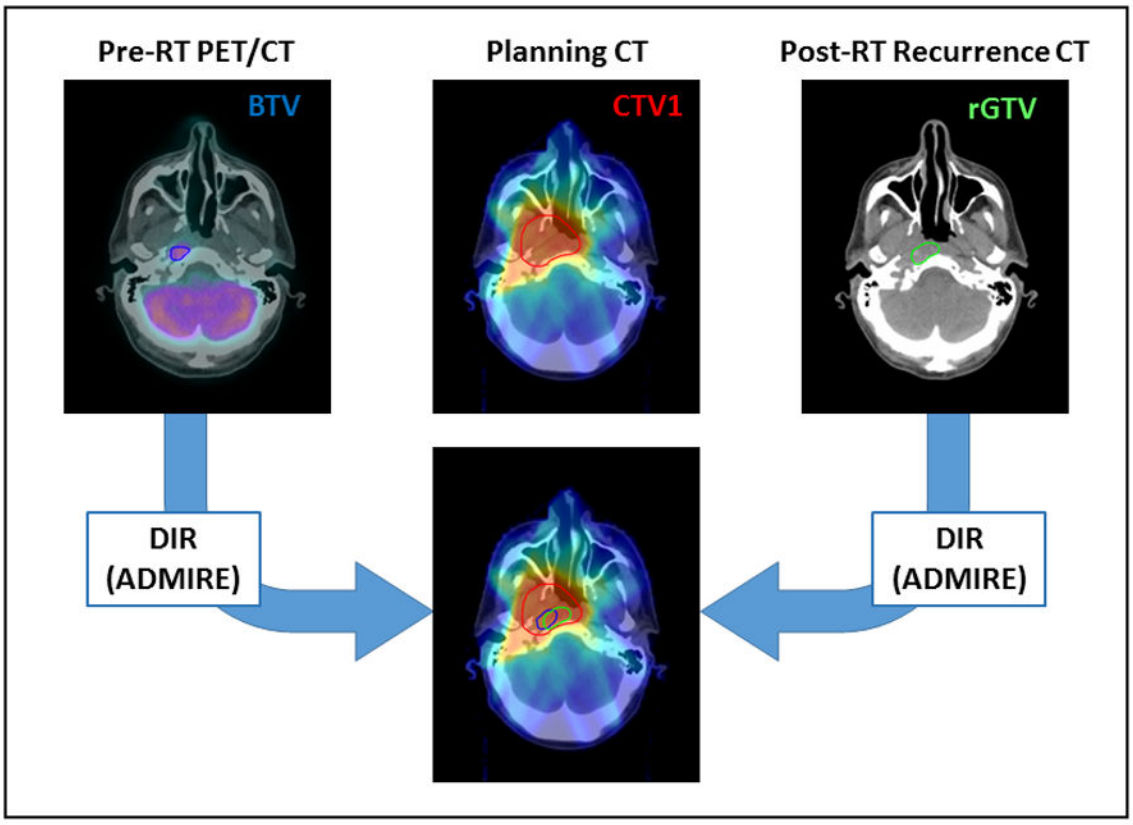

Figure 1.
This diagram depicts the workflow methodology of the current study.

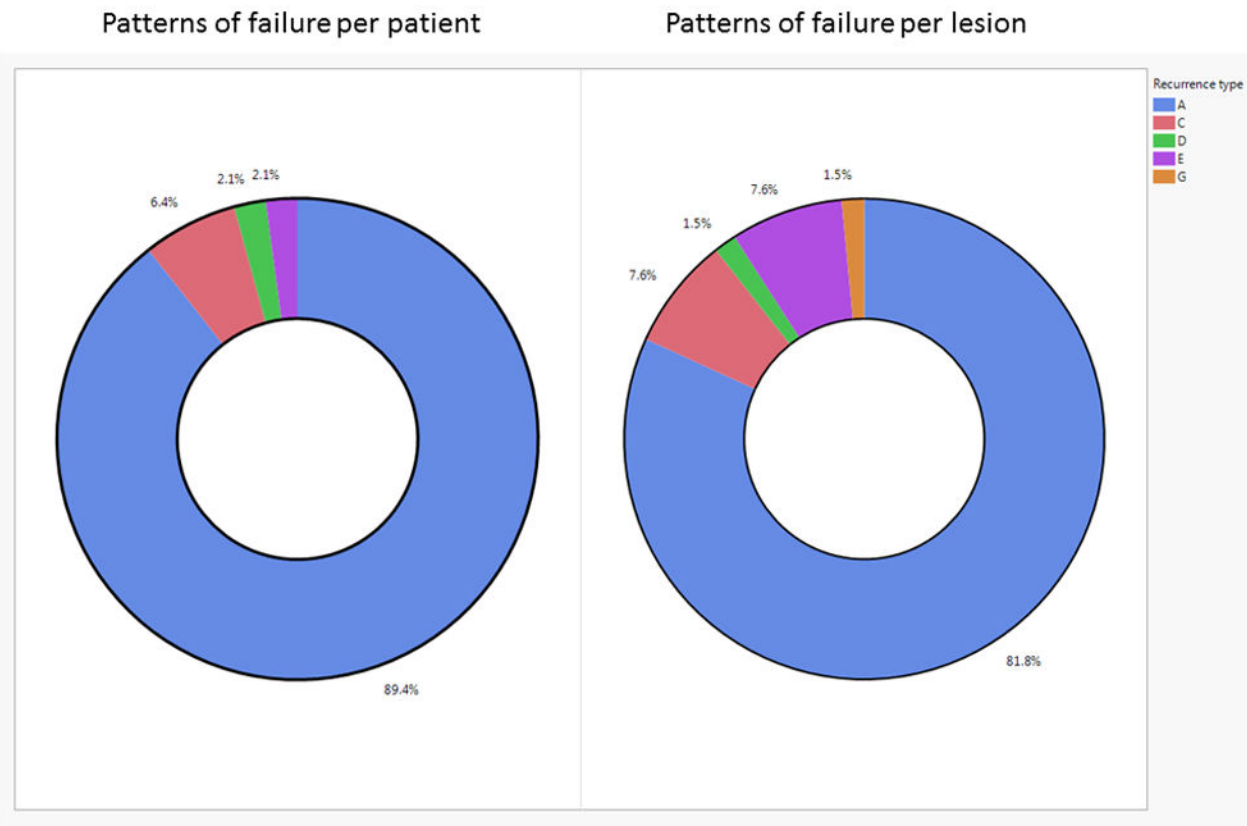

Figure 2.
Pie charts of the patterns of failure classification.

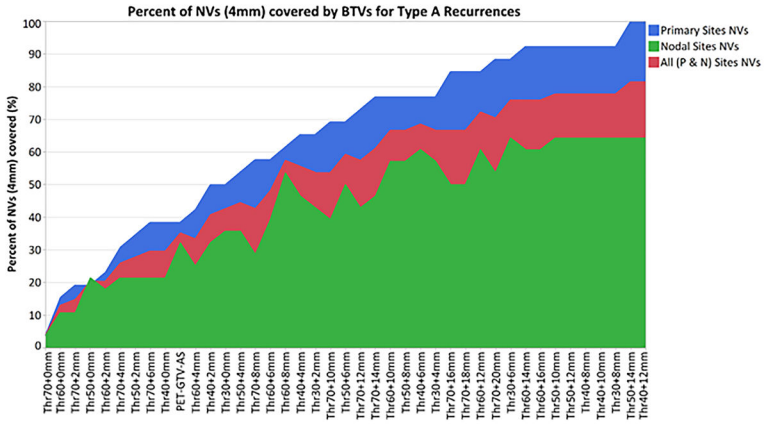

Figure 3.

This figure shows the percent of type A recurrences' origin covered by Boost Volume when considering the nidus volume created by adding a 4 mm radius. Boost volumes with an average volume greater than 100% of CTV1 are not shown as per our criteria, BTV volume must be less than CTV1 volume. Recurrent lesions were classified per their anatomical location, and coverage per class (n. of primary rGTVs=26, n. of nodal rGTVs=28, total type A's rGTVs=54) are shown in this figure.

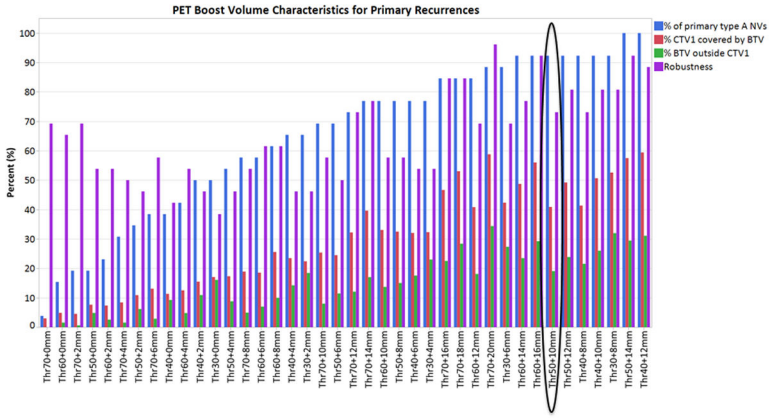

Figure 4.

This figure shows the PET boost volume metrics used for determining the “best” boost volume. The blue bars show % of primary site nidus volumes covered per boost volume (100% is best, 0% is the worst). The red bars show the % of CTV1 that are being covered by BTV (less is better, we don’t want the whole CTV1 to be boosted). The green bars show the % of voxels of each boost volume that are outside the CTV1 (the idea is that we want the boost volume to be mostly inside the CTV1, so 0% is best and 100% is worst). Lastly, the purple bars represents each boost volume’s robustness. Robustness is calculated per volume by looking at the difference in coverage for different nidus radius. The higher the number the more robust the volume is. Boost volumes that are greater than CTV1 have been excluded. Volumes are ordered by increasing % of patients covered. BTV50+10mm had the best collective performance with highest possible NV coverage (92.3%), least relative volume to CTV1 (41%), least percent voxels outside CTV1 (19%), and reasonable robustness score (73%)

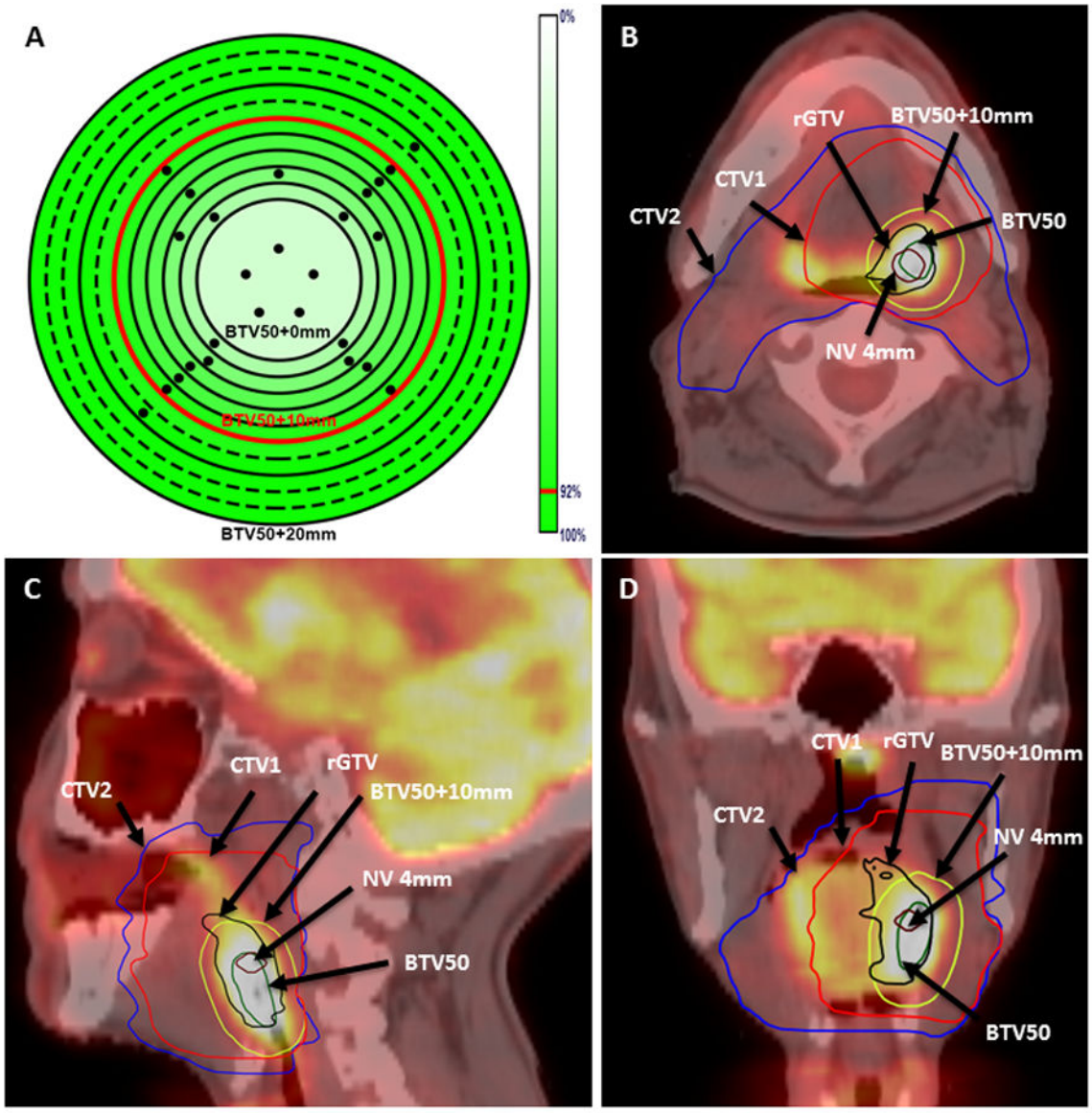

Figure 5.

Panel A shows a heat map of percent of lesions covered (4mm nidus) for volumes segmented using a 50% of SUVmax threshold value. The dots on Panel A represent patients with primary recurrences, whereas the different rings represent the different margins increasing from the center to the outer most ring by a 2 mm interval. Panels B–D show an example of a T2N2b left tonsillar patient with local recurrence at the primary site. The 4mm nidus volume (magenta), primary recurrence (black), BTV50 (green), BTV50+10mm (yellow), CTV1 (red), and CTV2 (blue) are highlighted.

Table 1

Patient, disease, and treatment characteristics

Variables	No. of patients (%)
Gender	
Male	42 (89%)
Female	5 (11%)
Smoking Status	
Smoker	32 (68%)
Non-smoker	15 (32%)
Primary Site	
Oropharynx	30 (64%)
Hypopharynx	7 (15%)
Oral cavity	1 (2%)
Nasopharynx	3 (6%)
Sinonasal	2 (4%)
Larynx	4 (9%)
T stage	
T1	7 (15%)
T2	18 (38%)
T3	9 (19%)
T4	13 (28%)
N stage	
N0	2 (4%)
N1	6 (13%)
N2a	4 (8%)
N2b	17 (36%)
N2c	13 (28%)
N3	5 (11%)
HPV status	
Positive	17 (36%)
Negative	4 (9%)
Unknown	26 (55%)
IMRT dose & fractionation	
Mean Dose (SD), in Gy	69.5 (1.5)
Mean n. of Fractions (SD)	33 (1.6)
Chemotherapy	
Induction	5 (11)
Concurrent	17 (36)
Induction and concurrent	20 (42)
No chemotherapy	5 (11)